Raytheon

ICE SURFACE TEMPERATURE

VISIBLE/INFRARED IMAGER/RADIOMETER SUITE ALGORITHM THEORETICAL BASIS DOCUMENT

Version 5: March 2002

Richard J. Sikorski
Kenneth A. Jensen

William Emery, Science Team Member
University of Colorado

RAYTHEON SYSTEMS COMPANY
Information Technology and Scientific Services
4400 Forbes Boulevard
Lanham, MD 20706

SBRS Document #: Y2405

EDR: ICE SURFACE TEMPERATURE

Doc No: Y2405

Version: 5

Revision: 2

	Function	Name	Signature	Date
Prepared by	EDR Developer	R. SIKORSKI		1/18/02
Approved by	Reviewer	P. KEALY		1/31/02
Approved by	Surface Temperature IPT Lead	R. SIKORSKI		2/11/02
Approved by	Chief Scientist	S. MILLER		2/15/02
Released by	Algorithm IPT Lead	P. KEALY		2/15/02

TABLE OF CONTENTS

Page

LIST OF FIGURES

Page

LIST OF TABLES

Page

GLOSSARY OF ACRONYMS

AMSR	Advanced Microwave Scanning Radiometer
ARP	Application-Related Product
ATBD	Algorithm Theoretical Basis Document
ATSR	Along Track Scanning Radiometer
AVHRR	Advanced Very High Resolution Radiometer
CGS	Centimeter-Gram-Second
ECMWF	European Center for Medium-Range Weather Forecast
EDR	Environment Data Record
HSR	Horizontal Spatial Resolution
ICD	Interface Control Document
IP	Intermediate Product
IR	Infrared
IST	Ice Surface Temperature
LOWTRAN	Low-resolution Transmission Model
LUT	Look Up Table
LWIR	Longwave Infrared
MAS	Modis Airborne Simulator
MODIS	Moderate Resolution Imaging Spectroradiometer
MODTRAN	Moderate Resolution Atmospheric Radiance and Transmittance Model
MOSART	Moderate Spectral Atmosphere Radiance and Transmittance
NCEP	National Centers for Environment Prediction
NEdT	Noise Equivalent Delta Temperature
NPOESS	National Polar-orbiting Operational Environmental Satellite System
NPP	NPOESS Preparatory Program
P^3I	Pre-Planned Product Improvements
RMS	Root Mean Square
SBRS	Santa Barbara Remote Sensing
SDR	Sensor Data Record
SSM/I	Special Sensor Microwave Imager
SST	Sea Surface Temperature

ST	Surface Temperature
TOA	Top Of Atmosphere
VIIRS	Visible/Infrared Imager/Radiometer Suite
VZA	Viewing Zenith Angle

ABSTRACT

This is the Algorithm Theoretical Basis Document (ATBD) for Ice Surface Temperature (IST) retrieval from infrared (IR) signals received by the National Polar-orbiting Operational Environmental Satellite System (NPOESS) Visible/Infrared Imager/Radiometer Suite (VIIRS), for retrieval of the VIIRS IST Environmental Data Record (EDR) and the IST Intermediate Product (IP).

This document describes the theoretical basis and development process of the IST algorithm being developed by the NPOESS algorithm team. The VIIRS IST algorithm is based on a water vapor correction method. It utilizes radiances from two of the VIIRS Longwave Infrared (LWIR) channels. The VIIRS IST split window algorithm meets the VIIRS IST uncertainty requirement of 0.5 K.

The major error sources for IST retrievals are the atmospheric correction and VIIRS sensor performance. There are a number of difficulties in evaluating the accuracy of satellite estimates of IST. These include the difficulty in distinguishing the snow/ice surface from clouds, and the lack of high-quality *in situ* data. The major constraints for the surface temperature algorithm are instrument Noise Equivalent Delta Temperature (NEdT) for each band; instrument calibration; and the availability and quality of the surface calibration/validation observations.

1.0 INTRODUCTION

1.1 PURPOSE

This document describes the theoretical basis and development process of the IST algorithms, for retrieval of the VIIRS IST EDR and the IST Intermediate Product (IP).

1.2 SCOPE

The IST algorithms described in this ATBD will be used to routinely retrieve IST from VIIRS. Section 2 of this ATBD provides an overview of the IST algorithm. A description of the algorithm and the development process are presented in Section 3. Section 3 also addresses the error budget, algorithm sensitivity, and validation. Constraints, assumptions, and limitations are discussed in Section 4, and Section 5 presents all citation references in this document.

1.3 VIIRS DOCUMENTS

This document contains references to other Raytheon VIIRS documents, which are given in italicized brackets:

[SS154640-001] VIIRS System Specification

[PS154640-101] VIIRS Sensor Specification

[Y2386] VIIRS Sea Surface Temperature ATBD

[Y2469] VIIRS Context Level Software Architecture document

[Y2471] - VIIRS Aerosol Module Level Software Architecture

[Y2479] - VIIRS Build SDR Module Level Software Architecture

[Y2473] VIIRS Surface Temperature Module Level Software Architecture document

[Y3261] - VIIRS Radiometric Calibration ATBD

[Y3277] - VIIRS Aerosol Module Level Interface Control Document

[Y10880] – VIIRS Surface Temperature IP Unit Level Detailed Design Document

[Y10881] – VIIRS Ice Quality Unit Level Detailed Design Document

[Y3282] – VIIRS Precipitable Water Unit Level Detailed Design Document

1.4 REVISIONS

This is the fifth version of this document, dated January 2002. Substantial contributions to prior versions of this document were made by Yimin Ji and Philip E. Ardanuy.

2.0 EXPERIMENT OVERVIEW

2.1 OBJECTIVES OF ICE SURFACE TEMPERATURE RETRIEVALS

Ice Surface Temperature is a crucial measure of the Arctic climate. It is a good indicator of the energy balance at the ice surface. The energy exchange between atmosphere and ice layer influences the global climate by controlling the mass balance. A long-term data set of IST can be used to detect and understand the greenhouse effect and climate changes in the polar region. For years the collection of IST has relied on *in situ* measurement from ships, manned ice camps and drifting buoys. The data coverage and our knowledge of the Arctic IST remains poor compared with the other part of the earth's surface. When sufficiently calibrated, satellite retrieval of IST provides this coverage.

Although much effort has gone into evaluating the accuracy of satellite measurement of sea surface temperature, there has been no comparable effort for IST. This is due to the considerably greater difficulty in distinguishing the ice surface from clouds and the lack of sufficient high quality *in situ* data. The current Root Mean Swuared (RMS) error of satellite retrieved IST is about 1 to 3 K (Yu *et al*., 1995; Key *et al.*, 1994). However, the IST has not been retrieved operationally. In general the moisture is lower in the polar atmospheres, although it is significant in many cases. The IST retrieval methods are split-window statistical methods. Due to the dry air over polar regions, it is often possible to retrieve IST from only one channel within these regions.

The overall scientific objective of the VIIRS IST retrievals is to provide improved measures of global and regional IST fields. The VIIRS IST EDR requires a 1.0 K measurement uncertainty. The requirements are met, provided accurate cloud/ice discrimination is available.

2.2 INSTRUMENT CHARACTERISTICS

The VIIRS sensor design is based on the NPOESS sensor requirements and EDR thresholds and objectives. VIIRS bands in the Longwave Infrared (LWIR) were placed to optimize their use for Sea Surface Temperature (SST). Bands in the LWIR are usually located near the maximum earth radiance. The influence of ozone and other atmospheric absorbers must be avoided. Figure 1 shows the Moderate Resolution Atmospheric Radiance and Transmittance Model (MODTRAN) simulated radiance at satellite height for the thermal infrared spectrum. There are a total of five standard atmospheres. There are two regions suitable for LWIR band selection: 8-9 μm and 10-13 μm. VIIRS LWIR bands are located in these two regions. Bands in the far-infrared also need to be placed where the atmosphere is most transparent. Figure 2 shows the MODTRAN simulated atmospheric transmittance for five standard atmospheres. It shows that the 10-13 μm region is one of the most transparent atmosphere windows for arctic atmospheres.

2.3 ICE SURFACE TEMPERATURE RETRIEVAL STRATEGY

A Cloud Mask, a Land/Ocean Mask, and a Snow/Ice mask are necessary to eliminate cloud contaminated pixels, land pixels, and ocean pixels. The IST algorithms are run only under confident clear and probably clear sky conditions. The brightness temperatures are calculated for the two bands for all suitable pixels within a region.

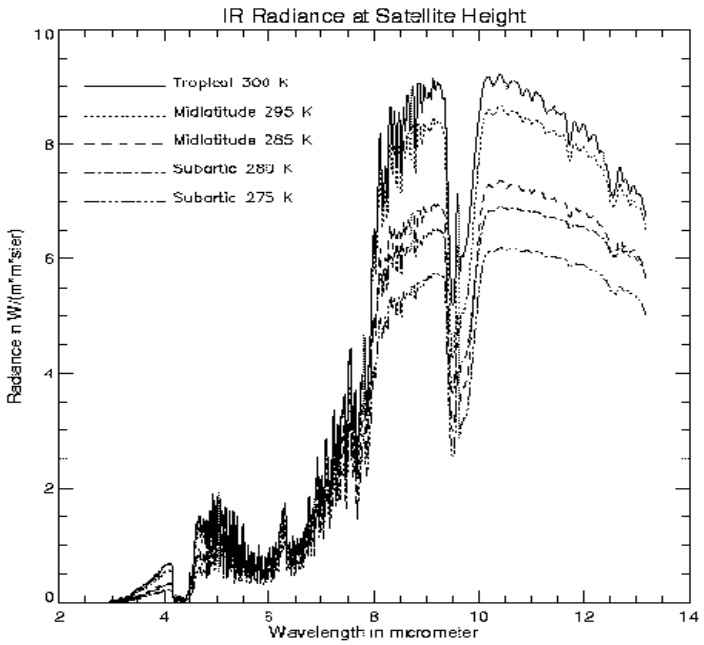

Figure 1. IR radiance at the satellite for five atmospheres simulated by MODTRAN.

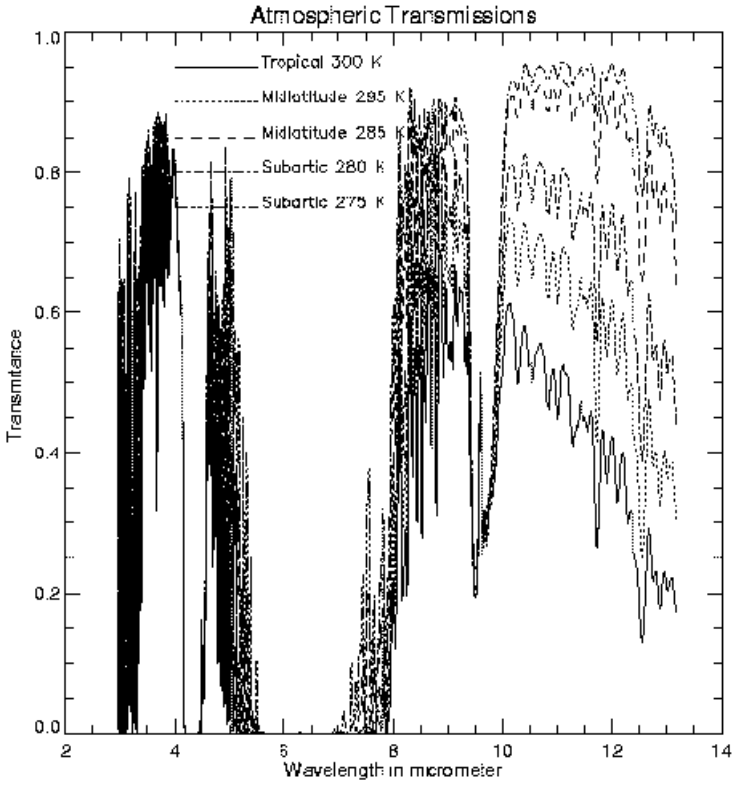

Figure 2. Atmospheric transmittance for five atmospheres.

3.0 ALGORITHM DESCRIPTION

3.1 PROCESSING OUTLINE

The VIIRS IST retrieval uses an Along Track Scanning Radiometer (ATSR) like regression method. Regression methods are initially assisted by the establishment of ancillary data and radiative transfer models. The coefficients of regression equations are obtained from simulation processes. Figure 3 depicts the processing concept for statistical IST retrieval.

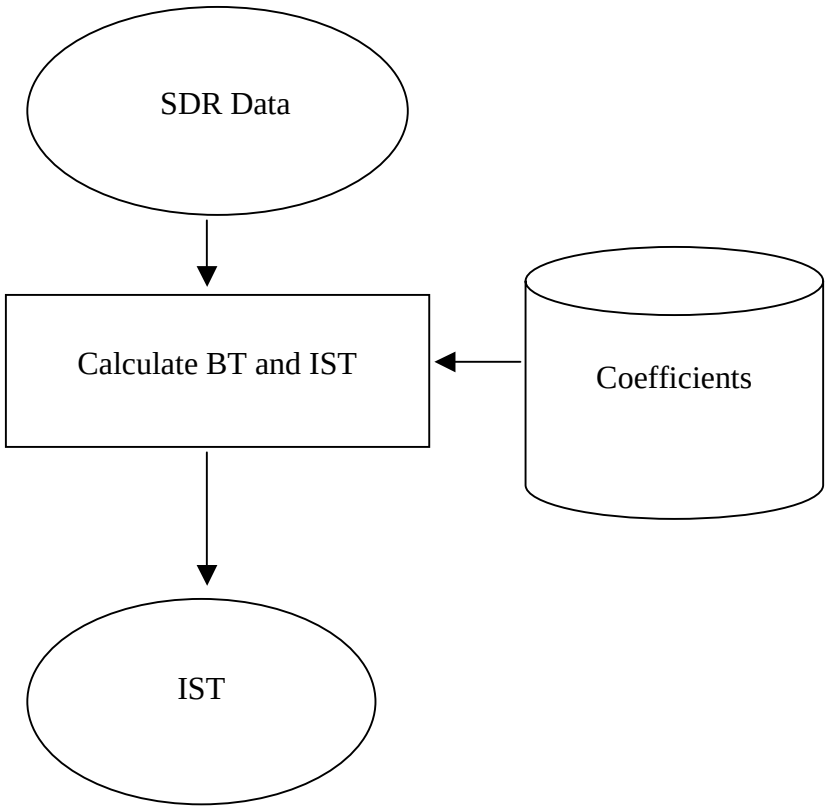

Figure 3. IST high level flowchart: regression method.

3.2 ALGORITHM INPUT

3.2.1 VIIRS Data

The VIIRS data presented in Table 1 are required input to the algorithm processing code.

Table 1. VIIRS data for the IST EDR

Input Data	Source of Data	Reference
Instrument (Band) Quality	VIIRS Sensor Data Record (SDR)	*[Y2479]*
Granule Range Flag	Ice Mask IP	*[Y10881]*
Brightness Temperature (M15, M16, I5)	VIIRS SDRs	*[Y2479], [Y3261]*
Solar/Sensor Angles	VIIRS SDRs	*[Y2479]*
Aerosol Optical Thickness (AOT)	Aerosol Optical Thickness IP	*[Y2471], [Y3277]*
Precipitable Water (PW)	Precipitable Water IP	*[Y3282]*
Cloud Mask	Cloud Mask IP	*[Y2412]*
Surface Temperature IP Parameters	Surface Temperature IP Look Up Tabl;e (LUT)	*[Y10880]*

Instrument (Band) Quality

The VIIRS EV_375M SDR will contain band I5 quality flags at imagery pixel resolution. Pixels with bad quality will not be processed. A RED quality flag will be set for these pixels. The VIIRS EV_750M SDR will contain band M15 and M16 quality flags at moderate pixel resolution. Imagery pixels nested within a moderate resolution pixel with bad quality will be processed by the fallback single band algorithm. A YELLOW quality flag will be set for these pixels.

Granule Range Flag

If the entire granule is out of the Horizontal Coverage range for all ice Application-Related Products (ARPs) and EDRs, a granule range flag will be set in the Ice Mask IP. In that case,

further processing of the granule will be bypassed. This will reduce the operational processing load, since most granules are out of range.

Brightness Temperatures

Brightness temperatures for the M15 and M16 bands are obtained from the VIIRS EV_750M SDR. Brightness temperatures for the I5 band are obtained from the VIIRS EV_375M SDR.

Solar / Sensor Angles

The Viewing Zenith Angle (VZA) is used in the split window algorithm (Equation A-6).

Aerosol Optical Thickness

Aerosol optical thickness is used for BT correction.

Precipitable Water

Precipitable water is used for BT correction.

Cloud Mask

The VIIRS cloud mask *[Y2412]* is expected to derive a status of confident clear / probably clear / probably cloudy / confident cloudy for each pixel, building on Moderate Resolution Imaging Spectroradiometer (MODIS) cloud mask heritage (Ackerman *et al.*, 1997). Pixels classified as "cloudy" will be excluded from further processing. Pixels classified as "probably cloudy" are also expected to be excluded. This determination must depend on an assessment of the cloud mask performance, particularly over snow and ice surfaces. Pixels classified as "probably clear" or as "confident clear" will be processed. The cloud mask will also supply a thin cirrus flag, which may be used for BT correction.

Surface Temperature IP Parameters

A set of input parameters will be obtained from a pre-set VIIRS Surface Temperature IP LUT. The parameters also include a switch determining whether to use the Cloud Mask IP or the Cloud Optical Thickness IP for cloud masking, another switch determining whether or not to apply BT corrections, and a weight factor (spectral fusion factor) for combining the M15 and M16 BTs (c.f. Equation A-7).

3.2.2 Non-VIIRS Data

The algorithm requires no input data from outside the VIIRS system.

3.3 THEORETICAL DESCRIPTION OF ICE SURFACE TEMPERATURE RETRIEVAL

3.3.1 Physics of the Problem

In clear sky conditions, the outgoing infrared spectral radiance at the top of atmosphere can be represented by:

$$L(\lambda,\mu)=\tau(\lambda,\mu)\varepsilon(\lambda,\mu)B(\lambda,T_s)+L_a(\lambda,\mu)+L_s(\lambda,\mu,\mu_0,\varphi_0) \\ +L_d(\lambda,\mu,\mu_0,\varphi_0)+L_r(\lambda,\mu,\mu_0,\varphi_0) \quad (1)$$

Where τ is the transmissivity, ε the surface spectral emissivity, B the Plank function, L_a the thermal path radiance, Ls the path radiance resulting from scattering of solar radiation. L_d is the solar radiance and L_r the solar diffuse radiation and atmospheric thermal radiation reflected by the surface. λ is the wavelength. $\mu=\cos(\theta)$, $\mu_o=\cos(\psi)$, where θ is the satellite zenith angle, ψ the solar zenith angle. φ_o is azimuth angle.

The wavelength is the wavelength center of a narrow interval because there is no way to measure the exact monochromatic signal as a continuous function of wavelength by satellite sensors. Equation 1 can be used in the 3-14 μm range. It requires complete calculations of the atmospheric radiative transfer to determine the values of all terms on the right side. This equation has been used in many atmospheric radiation models including the Low-resolution Transmission Model (LOWTRAN) (Kneizys *et al*., 1988), MODTRAN (Berk *et al*., 1987), and the Moderate Spectral Atmosphere Radiance and Transmittance (MOSART) (Cornette *et al*., 1994).

The satellite infrared radiance can be corrected for atmospheric absorption in the water vapor bands by utilizing a split window technique. In the following discussion, we outline a theoretical basis for the split window method.

For LWIR bands, L_d, L_s and L_r are negligible. Therefore, only the first two terms on the right side of the above equation are important. In this case, if we ignore the change of emissivity over the ocean, the radiance error introduced by the atmosphere ΔL can be represented by:

$$\Delta L = B(\lambda,T_s)-L(\lambda,\mu)=B(\lambda,T_s)-\tau(\lambda,\mu)B(\lambda,T_s)-L_a(\lambda,\mu) \\ =-\int_1^{\tau(\lambda,\mu)}B(\lambda,T_s)d\tau(\lambda,\mu,p)+\int_1^{\tau(\lambda,\mu)}B(\lambda,T_p)d\tau(\lambda,\mu,p) \quad (2) \\ =-\int_1^{\tau(\lambda,\mu)}(B(\lambda,T_s)-B(\lambda,T_p))d\tau(\lambda,\mu,p)$$

From the Planck function we find:

$$\Delta L=\frac{\partial B}{\partial T}\Delta T=\frac{\partial B}{\partial T}(T_s-T_\lambda) \quad (3)$$

For an optically thin gas the following approximations can be made:

$$d\tau = d\{exp(-k\lambda L)\} = -k\lambda dl \tag{4}$$

Where k_λ is the absorption coefficient and l is the optical path-length. If we assume that the Planck function is adequately represented by a first order Taylor series expansion in each channel window, then:

$$B(\lambda,T_s) - B(\lambda,T_p) = \left.\frac{\partial B(\lambda,T_p)}{\partial T}\right|_{T_s} (T_p - T_s) \tag{5}$$

Substituting Equations 3, 4, 5 into Equation 2, we obtain:

$$T_s - T_\lambda = k_\lambda \int_1^\tau (T_s - T_p) dl \tag{6}$$

Therefore, if we pick two spectral regions of the atmosphere, we have two linear equations with different k_λ to solve simultaneously.

For example, if we consider two channels as λ=1 and λ=2, then we get:

$$T_s\text{-}T_1 = -(T_s\text{-}T_2)k_1/k_2 \tag{7}$$

Figure 4 shows the relationship between T_s-T_{11} and T_s-T_{12} from MODTRAN simulations. The brightness temperature at the 10.8 μm (T_{11}) band is higher than that at the 12 μm band (T_{12}). However, the relationship between T_s-T_{11} and T_s-T_{12} is rather linear. The maximum difference is only about 3 K.

In general, the ice surface temperature can be represented as:

$$\mathbf{T_s} = \mathbf{CT_b} \tag{8}$$

The coefficient vector **C**, relating observed brightness temperatures to IST, is determined using regression methods by solving:

$$\mathbf{C} = \mathbf{YX}^T(\mathbf{XX}^T + k\mathbf{I})^{-1} \tag{9}$$

The **Y** matrix contains a large number of training IST, and the **X** matrix contains brightness temperatures from VIIRS LWIR channels. In general, the **X** matrix may include non-linear terms.

Because the atmospheric correction term is small, it is often possible to use only one channel to retrieve IST. Figure 5 shows the relationship between IST and the brightness temperature at the 12 μm band. The relationship is linear.

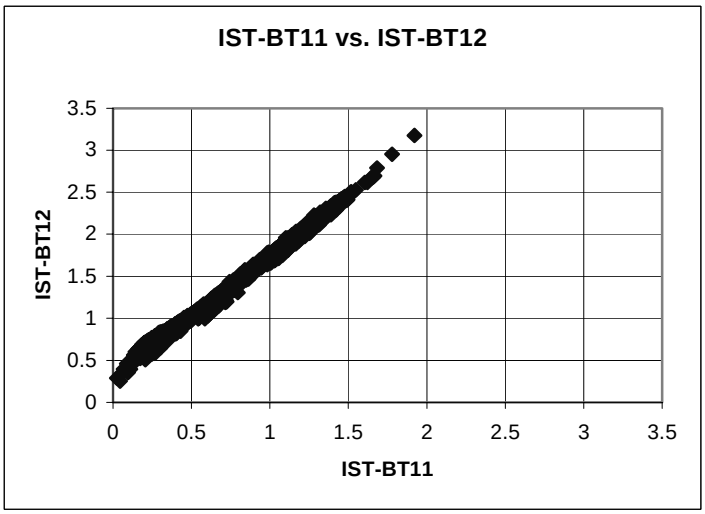

Figure 4. The relationship between temperature deficits at 10.8 µm band and at 12 µm band.

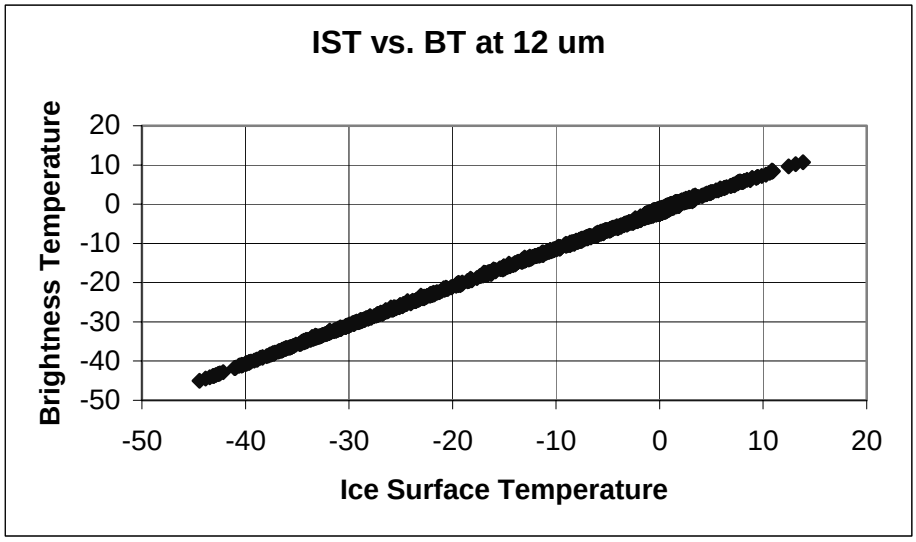

Figure 5. The relationship between IST and brightness temperature at the 12 µm band.

Currently, the IST uncertainty from the regression algorithm is about 1 to 3 K.

3.3.2 Mathematical Description of the Algorithm

3.3.2.1 Split Window Regression

The VIIRS IST algorithm is based on statistical methods. Traditional statistical methods for satellite IST retrieval are linear multi-channel regression methods. The following regression methods are used in the VIIRS IST retrieval:

Split window (10.8 + 12 μm bands, from the **Advanced Very High Resolution Radiometer (**AVHRR) method, Yu et al., 1995) (VIIRS IST baseline algorithm):

$$IST = a_o + a_1 T_{11} + a_2 (T_{11} - T_{12}) + a_3 (\sec(z) - 1) \quad (10)$$

One channel (12 μm band). (VIIRS IST fallback algorithm):

$$IST = a_o + a_1 T_{12} + a_2 (\sec(z) - 1) \quad (11)$$

Satellite-measured radiance is a function of the atmospheric profiles and surface properties. For the Infrared (IR) window and water vapor channels, the radiance over oceans at the top of the atmosphere is mainly a function of the surface temperature and the temperature and moisture profiles. One can choose a few channels (e.g., 3 channels) for which only the main structures of the temperature and moisture profiles are required to obtain ice surface temperature.

3.3.2.2 Calibrated Top Of Atmosphere (TOA) Brightness Temperatures

The blackbody radiance (R) function is

$$R = 2 h \nu^3 / [c^2 (\exp\{-h\nu/kT\} - 1)] \quad (12)$$

where ν is the wavenumber (cm^{-1}), h is the Planck constant, c is the speed of light, k is Boltzman's constant, and T is the temperature in Kelvin.

Equation 12 can be written as

$$R = c_1 \nu^3 / [c^2 (\exp\{-c_2 \nu/T] - 1)] \quad (13)$$

where c_1 and c_2 are two blackbody constants equal to 0.01191071 and 1.438838 respectively using Centimeter-Gram-Second (CGS) units.

This can be solved for the brightness temperature (T or T_b) to give:

$$T_b = c_2 \nu / \ln(1 + c_1 \nu^3 / R) \quad (14)$$

3.3.3 Archived Algorithm Output

IST is produced as an EDR according to the system specification, and in addition as a imagery resolution Surface Temperature (ST) IP. (See Appendix A.)

3.3.4 Variance and Uncertainty Estimate

IST retrieval uncertainty is determined by many factors, including atmospheric correction, the surface state, and sensor performance. For example, the surface state may be snow cover or melt pond, which have significantly different radiometric properties. And there are a number of error sources in sensor performance, such as sensor noise, calibration error, geolocation, and band-to-band registration.

The data set used to estimate the IST uncertainty and accuracy is a global snapshot of surface temperature at 2.5^{o} by 2.5^{o} resolution supplied by the National Centers For Environment Prediction (NCEP), with matching atmospheric profiles. The data were used to simulate the Top Of Atmosphere (TOA) radiance.

In Figure 6, the upper panel shows the global snapshot of IST at 00Z July 1, 1993 and the middle panel shows the retrieved IST. The lower panel shows the difference. The NEdT values are about 0.1 K for the split window (SBRS baseline sensor specification). The root mean square (RMS) error is about 0.16 K at this noise level without considering any absolute calibration errors. The maximum error is 0.74 K in daytime and 0.46 K in nighttime.

The retrieval error is a function of satellite viewing angles and surface temperature values. In Figure 7, the upper panel shows the IST precision as a function of satellite zenith angle and surface temperature. A 0.2 K absolute calibration error was assumed in this retrieval. The algorithm used is the split window regression method. The precision error is less than 0.3 K for most satellite zenith angles and temperatures. The middle panel shows the IST accuracy error.

The accuracy is generally better than 0.2 K. The lower panel shows the RMS error. The RMS error is less than 0.3 K for higher temperatures and most of the satellite viewing angles. For large zenith angles and lower surface temperatures, the uncertainty is larger, but still less than 0.5 K.

Figure 8 shows the IST precision, accuracy and uncertainty from the single band algorithm. The errors are larger in this algorithm than that in the split window algorithm. But the errors are still less than 0.5 K, except for large satellite viewing angles. These results are relevant for the ST IP at imagery resolution. (See Appendix A.)

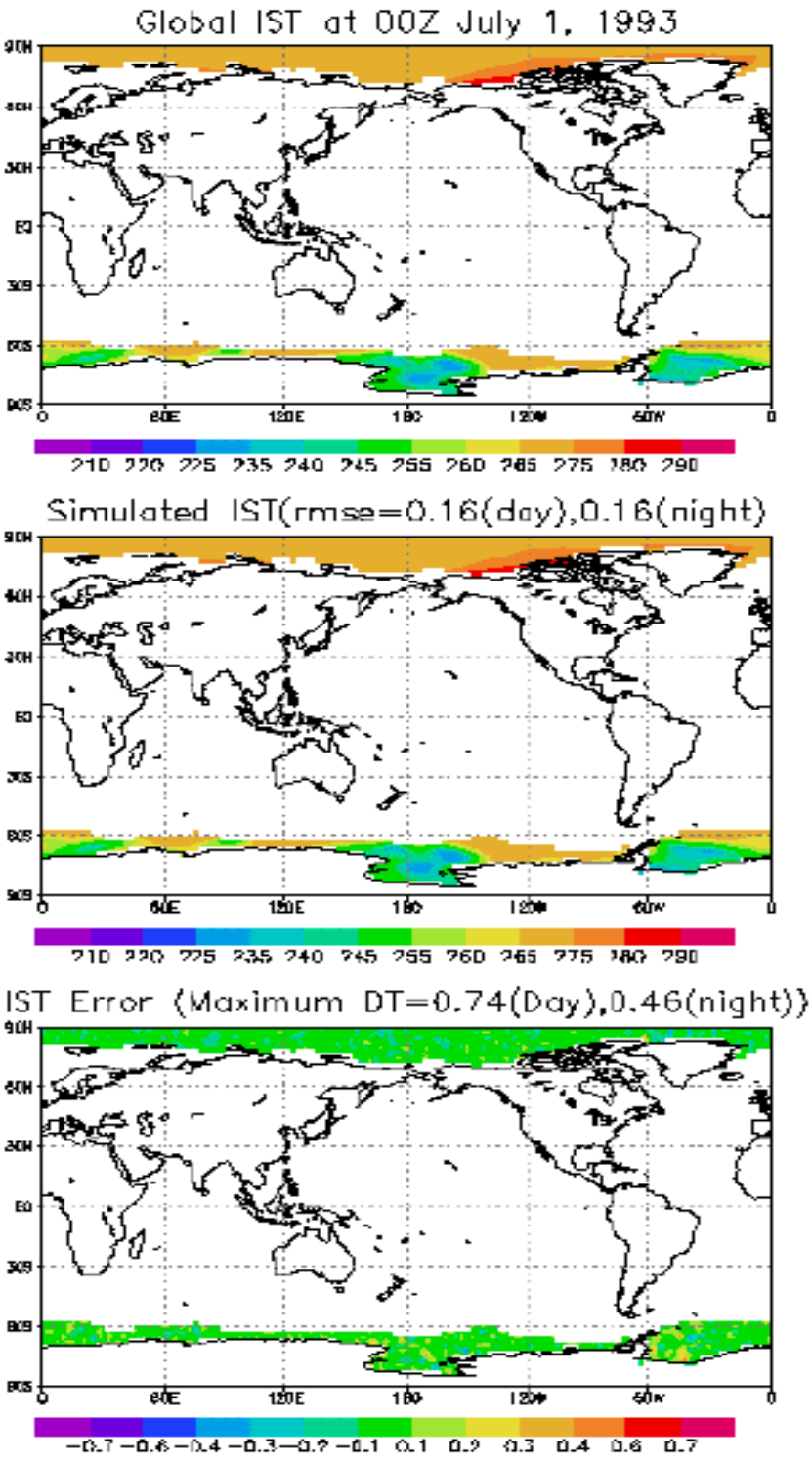

Figure 6. Upper panel: Global IST field. Middle panel: The retrieved IST values. Lower panel: The difference between the IST values.

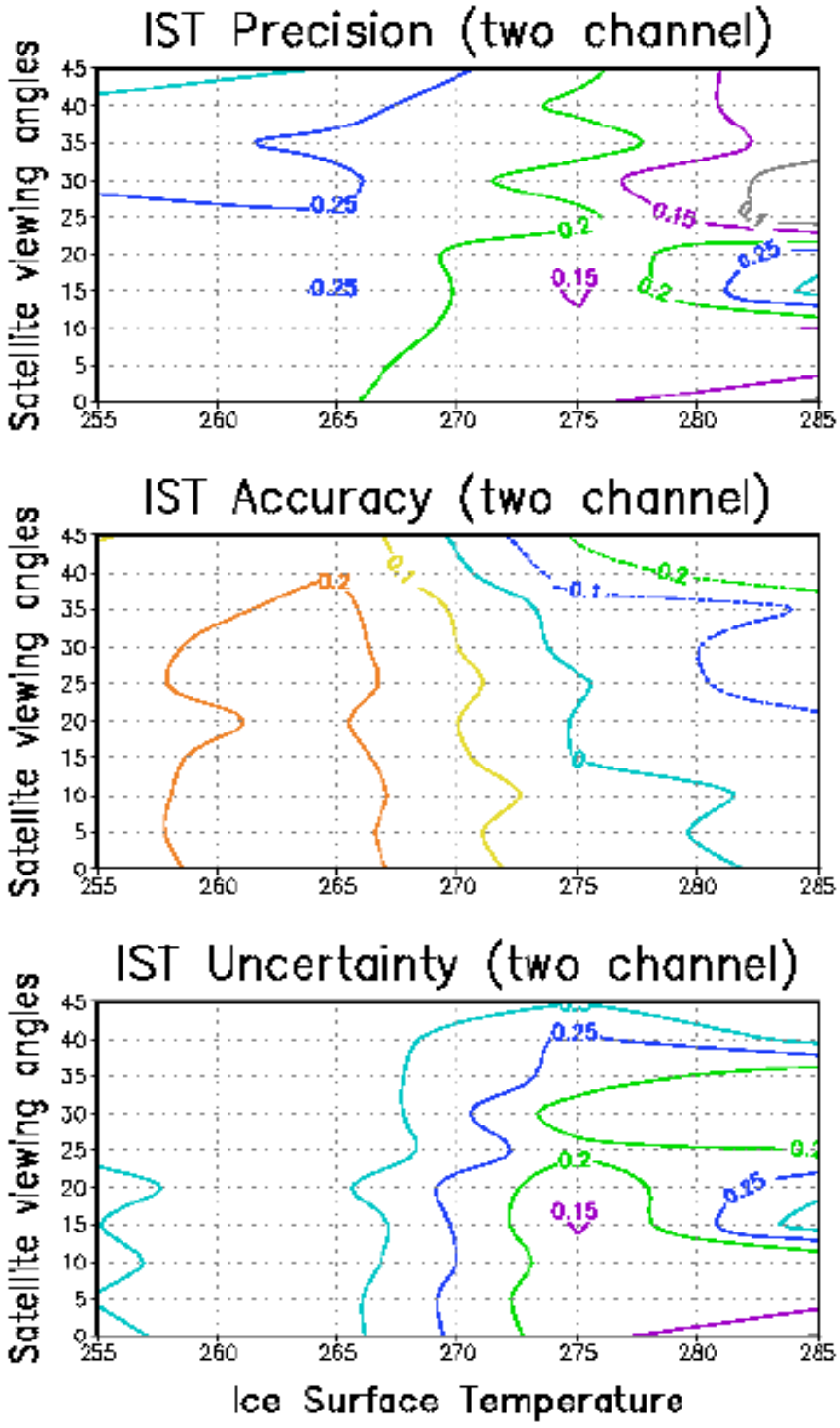

Figure 7. IST precision, accuracy, and uncertainty derived from the split window algorithms.

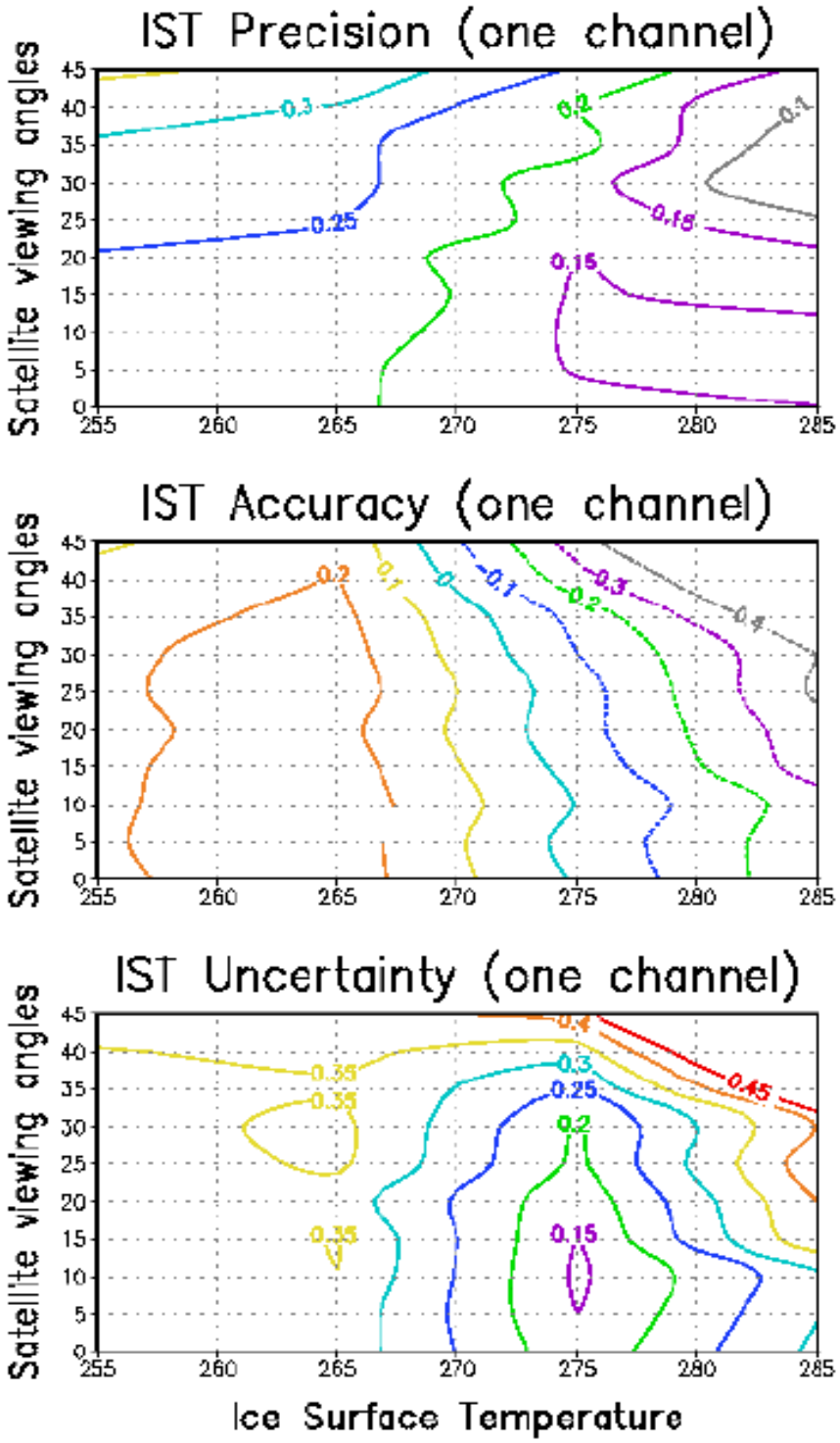

Figure 8. IST precision, accuracy, and uncertainty derived from the single band algorithms.

3.4 ALGORITHM SENSITIVITY STUDIES

3.4.1 Ice Water Mixing

Pixels which contain both ice and water are a major geophysical source of error, due to the significantly different radiometric properties of these surfaces. To estimate the error for the mixed region, both the SST algorithm and the IST algorithm were applied to two Modis Airborne Simulator (MAS) scenes. In Figure 9, the left panel shows the ice surface temperature map, the middle panel shows the map of sea surface temperature and the right panel shows the difference. The difference map indicates that the surface temperatures retrieved using the SST algorithm are generally higher than those derived from the IST algorithm, but the difference is smaller (<0.5 K) over the ice surface. Over water, the difference can be as high as 1 K. Figure 10 is similar to Figure 9, but for another scene. The result is similar to that of the previous scene.

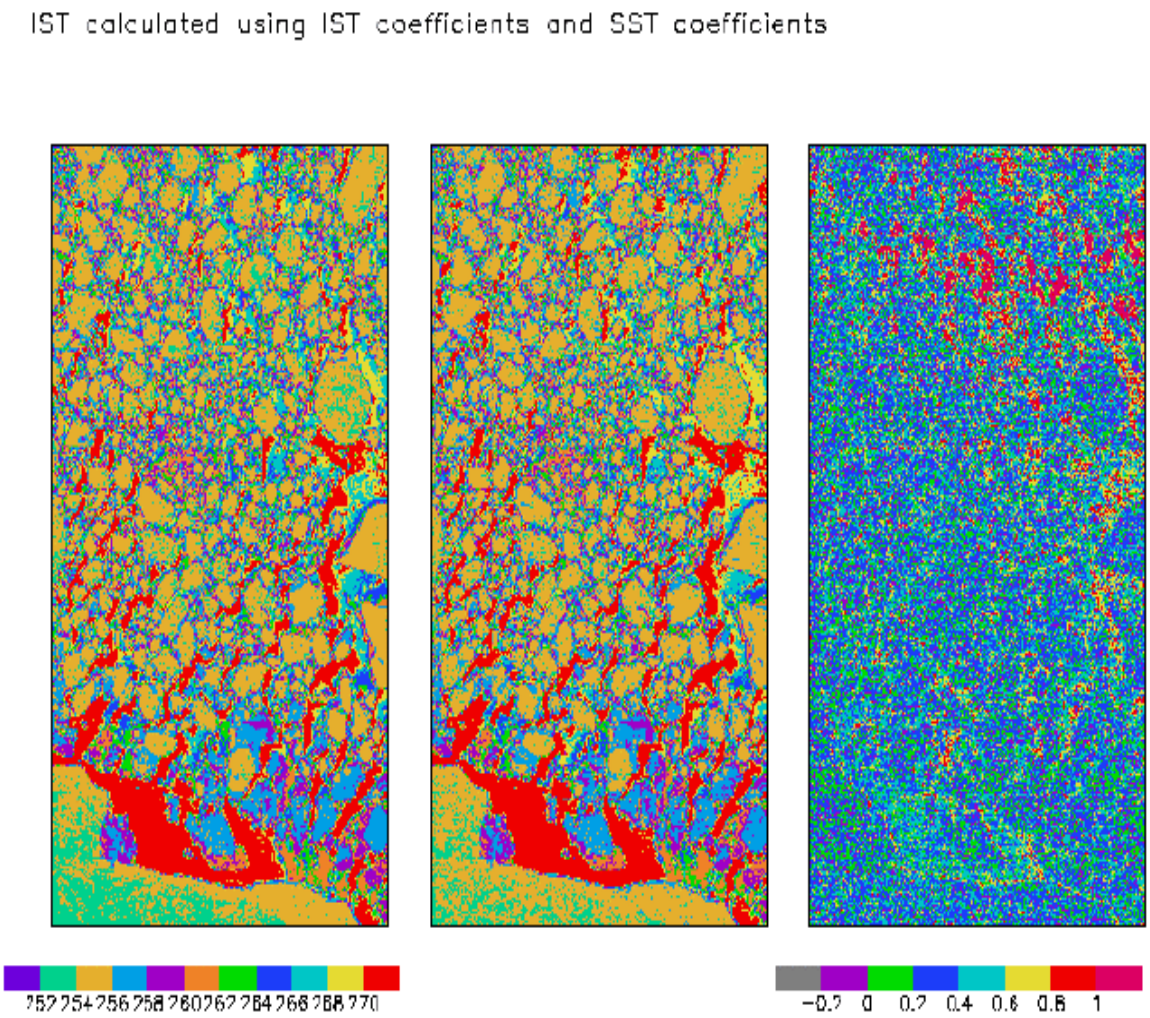

Figure 9. Left panel is the surface temperature derived using IST algorithm, middle is derived from the SST algorithm, and the right is the difference.

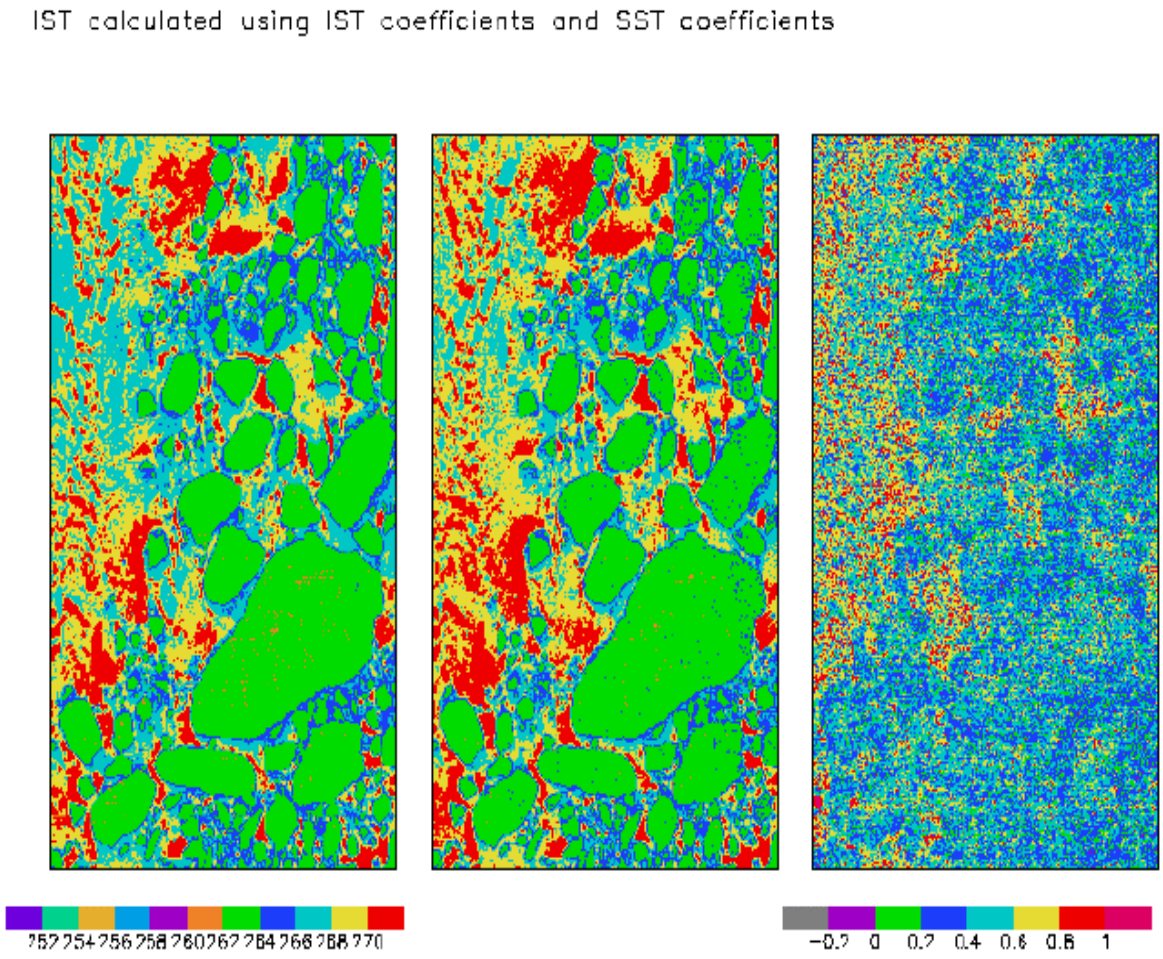

Figure 10. Left panel is the surface temperature derived using the IST algorithm, middle is derived from the SST algorithm, and the right is the difference.

3.5 PRACTICAL CONSIDERATIONS

3.5.1 Numerical Computation Considerations

In order to retrieve IST within an operational timeframe, statistical algorithms that meet quality requirements have been developed that are much quicker than physical modeling methods. Pre-generated LUTs are used to speed processing yet retain flexibility.

3.5.2 Programming and Procedural Considerations

The simplicity of all the algorithms described in this document translates into very small amounts of code using basic mathematical routines. Computationally intensive processes are performed offline, with results delivered as re-generated LUTs. VIIRS Phase II efforts are largely software-focused, and the methodology for this development work is based on sound and proven principles, as discussed in the VIIRS Algorithm Software Development Plan *[Y6635]*. The present maturity of the VIIRS software is detailed in the VIIRS Algorithm Software Maturity Assessment document *[Y6661]*. The maturity and remaining Phase II tasks for the algorithms themselves is summarized in the VIIRS Algorithm/Data Processing Technical Report *[Y7040]*. The software designs relevant to the IST Unit are summarized in the VIIRS Context Level Software Architecture *[Y2469]*, Surface Temperature Module Level Software Architecture *[Y2473]*, and Ice Surface Temperature Unit Level Detailed Design *[Y2503]*. These designs are tested at the system level as described in the most recent versions of the VIIRS Software Integration and Test Plan *[Y3236]*, Algorithm Verification and Validation Plan *[Y3237]*, and System Verification and Validation Plan *[Y3270]*. A summary of the ultimate strategy for operational application of the system of VIIRS algorithms is provided in the VIIRS Operations Concept document *[Y2468]*. The VIIRS Interface Control Document (ICD *[Y2470]*) provides more detail on the specifics of ancillary data requirements for Vegetation Index and other VIIRS products.

3.5.3 Configuration of Retrievals

Adjustable parameters for the retrieval of the IST products allow post-launch updating of regression coefficients. The flexibility built into the architecture also allows easy implementation of future P^3I developments.

3.5.4 Quality Assessment and Diagnostics

A number of parameters and indicators are reported in the IST product as retrieval diagnostic flags. Statistical information is reviewed for quality assessment. Table 2 lists the available quality flags. The final list of delivered flags will be determined in the operational environment.

Table 2. VIIRS IST Quality Flags

VIIRS IST flags	bits
Land/Water Background	3
Cloud Detection	2
IST Quality	2
spare	1

3.5.5 Exception Handling

Cloud pixels identified by the cloud mask are skipped and flagged. Pixels with bad radiance data are also skipped and flagged.

3.6 ALGORITHM VALIDATION

3.6.1 Pre-Launch Validation

The atmospheric correction algorithm coefficients will be derived pre-launch by radiative transfer modeling to simulate the VIIRS infrared channel measurements. Selected radiosondes from the operational network stations or field campaigns will be used in VIIRS simulations for the development of the atmospheric correction algorithm. Measurements from the operational surface drifting and fixed buoy programs will be used to characterize the surface temperature fields and to validate the atmospheric correction algorithms. The assimilated meteorological fields provided by NCEP and European Center for Medium-Range Weather Forecast (ECMWF) provide a valuable description of the marine atmosphere and surface temperatures. These fields will be used in conjunction with the radiative transfer modeling to simulate the VIIRS measurements, to validate the radiosonde data and to provide direct input to the radiative transfer modeling process.

Measurements from AVHRR, ATSR, and MODIS will be used in the pre-launch phase to study the error characteristics of the IST retrieval.

3.6.2 Post-Launch Validation

The infrared measurements are calibrated by using measurements of cold space and an on-board black body target. This produces radiance in the spectral intervals defined by the system response functions of each channel. These calibrated radiances can be converted to TOA brightness temperatures. To derive IST from the calibrated radiance at TOA, it is necessary to correct the effects of the intervening atmosphere.

The post-launch validation activities are important to test and improve the IST retrieval algorithm. The best retrieval accuracy can be achieved by developing comprehensive in situ data sets that provide adequate sampling of the atmospheric conditions and IST, including long-term studies to reveal sensor drift and the effects of episodic atmospheric changes.

4.0 ASSUMPTIONS AND LIMITATIONS

A major limitation of the VIIRS Ice Surface Temperature retrieval is that it can only be done under clear sky conditions. The accuracy of the retrieval is dependent on accurate cloud/ice discriminations.

5.0 REFERENCES

Berk, A., L. S. Bemstein, and D. C. Robertson (1987). MODTRAN: A moderate resolution model for LOWTRAN. Rep. GLTR-89-0122, Burlington, MA: Spectral Sciences, Inc.

Cornette, W. M., P. K. Acharya, D. C. Robertson, and G. P. Anderson (1994). Moderate spectral atmospheric radiance and transmittance code (MOSART). Rep. R-057-94(11-30), La Jolla, CA: Photon Research Associates, Inc.

Key, J., J. A. Maslanik, T. Papakyriakou, M. C. Serreze, and A. J. Schweiger (1994). On the validation of satellite-derived sea ice temperature. *Arctic*, 47, 280-287.

Kneizys, F. X., ., E. P. Shettle, L. W. Abreu, J. H. Chetwynd, G. P. Anderson, W. O. Gallery, J. E. A. Selby, and S. A. Clough (1988). Users guide to LOWTRAN7. Rep. AFGL-TR-88-0177, Bedford, MA: Air Force Geophys. Lab.

Yu, Y., D. A. Rothrock, and R. W. Lindsay (1995). Accuracy of sea ice temperature derived from the advanced very high resolution radiometer. *J. Geophys. Res.*, 100, 4525-4532.

APPENDIX A: SURFACE TEMPERATURE INTERMEDIATE PRODUCT

A.1.0 INTRODUCTION

A.1.1 PURPOSE

This appendix provides the theoretical basis for the Surface Temperature IP retrieval from IR signals received by the NPOESS VIIRS. The Surface Temperature IP is produced as required input data for the VIIRS Snow-Ice Module.

The baseline algorithm, based on a water vapor correction method, is adapted from the VIIRS algorithm for the IST EDR retrieval. It will utilize radiances from two of the VIIRS LWIR bands at moderate spatial resolution plus the VIIRS LWIR imagery resolution band, to derive surface temperature at imagery resolution. The fusion of moderate resolution bands with the imagery resolution band is achieved by modeling their spectral response functions and spatial response functions. The fallback algorithm uses a single band, and is most effective under dry atmospheres.

Calibration and algorithm validation are the two keys to ensure the performance of the algorithm. Both pre-launch and post-launch activities are discussed in this document. The validation of the VIIRS IST algorithm is discussed in Section A.3.6 of this document. Validation of the fusion approach will be TBD.

A.1.2 SCOPE

This appendix covers the theoretical basis for the derivation of the Surface Temperature IP, which consists of the surface temperature and associated quality flags at imagery resolution. The purpose and scope are described in Section A.1, while Section A.2 provides an overview of the retrieval objectives. Section A.3 describes the algorithm, its input data, the theoretical background, and some practical considerations. Section A.4 contains the algorithm performance analysis and error budget. Section A.5 contains the pre-launch and post-launch plan for verification and validation. Section A.6 contains assumptions and limitations.

A.1.3 VIIRS DOCUMENTS

This appendix contains references to other Raytheon VIIRS documents, which are given in italicized brackets:

[SS154640-001] VIIRS System Specification

[PS154640-101] VIIRS Sensor Specification

[Y2386] VIIRS Sea Surface Temperature ATBD

[Y2404] VIIRS Fresh Water Ice ATBD

[Y2409] VIIRS Sea Ice Age/Edge Motion ATBD

[Y2466] VIIRS Imagery ATBD

[Y2469] VIIRS Context Level Software Architecture document

[Y2471] - VIIRS Aerosol Module Level Software Architecture

[Y2472] - VIIRS Cloud Module Level Software Architecture

[Y2477] VIIRS Snow/Ice Module Level Software Architecture document

[Y2479] - VIIRS Build SDR Module Level Software Architecture

[Y2473] VIIRS Surface Temperature Module Level Software Architecture document

[Y3261] - VIIRS Radiometric Calibration ATBD

[Y3277] - VIIRS Aerosol Module Level Interface Control Document

[Y3278] - VIIRS Cloud Module Level Interface Control Document

[Y10880] – VIIRS Surface Temperature IP Unit Level Detailed Design Document

[Y10881] – VIIRS Ice Quality Unit Level Detailed Design Document

[Y3282] – VIIRS Precipitable Water Unit Level Detailed Design Document

A.1.4 REVISIONS

This is the first version of this appendix. It is appended to version 5 of the VIIRS Ice Surface Temperature ATBD, dated February 2002.

A.2.0 OVERVIEW

A.2.1 OBJECTIVES OF SURFACE TEMPERATURE RETRIEVAL AT IMAGERY RESOLUTION

The overall scientific objective of the VIIRS IST retrievals is to provide improved measures of global and regional IST fields. The VIIRS IST EDR requires a global horizontal cell size of 1 km at nadir with 1.0 K measurement uncertainty. The IST algorithm, described earlier in this document, retrieves surface temperature at the moderate resolution of the M15 and M16 bands.

The VIIRS ice products include the Sea Ice ARPs of the Imagery EDR *[Y2466]*, the Fresh Water Ice EDR *[Y2404]*, and the Sea Ice Age/Edge Motion EDR *[Y2409*]. All ice algorithms require surface temperature at imagery resolution as input data. Therefore, the software units that produce the VIIRS ice data products require surface temperature at imagery resolution. The VIIRS IST EDR is produced from moderate resolution data, so is not adequate for this purpose. The VIIRS Snow-Ice Module has therefore placed a requirement on the VIIRS system to provide an additional surface temperature product at imagery resolution.

A.2.2 INSTRUMENT CHARACTERISTICS

VIIRS moderate resolution bands in the LWIR were placed to optimize their use for SST. Two of these bands (M15 and M16) are used by the split window IST algorithm. The Surface Temperature IP algorithm will also use these bands for water vapor correction. In addition, the algorithm will use the imagery resolution LWIR band (I5). Band characteristics are indicated in Table A-1. Spectral response functions are illustrated in Figure A-1.

Table A-1. VIIRS bands used for Surface Temperature IP.

Band	Center Wavelength (μm)	Band Width [1] (μm)	Nadir resolution (m)	Ttyp	NEdT @ Ttyp (K)
M15	10.76	1.0	750	300 K	0.070
I5	11.45	1.9	375	210 K	1.5
M16	12.01	0.95	750	300 K	0.072

[1] FWHM

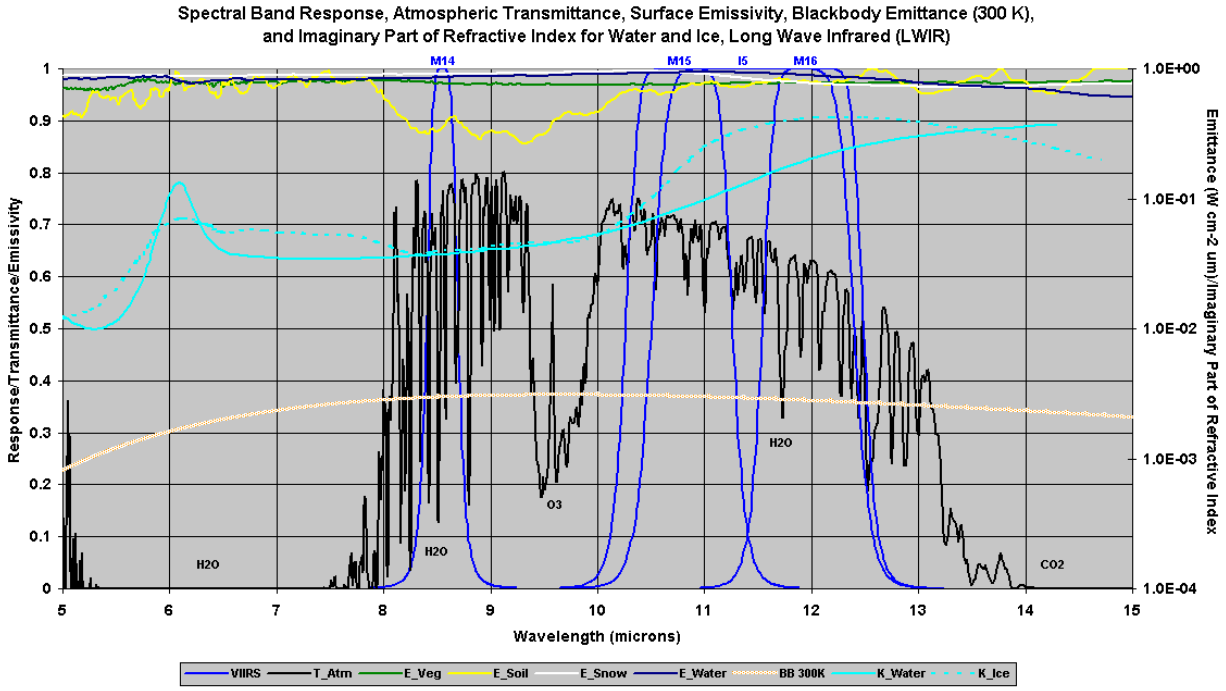

Figure A-1. Spectral response functions for VIIRS bands M15 (10.8 μm), I5 (11.5 μm), and M16 (12.0 μm).

A.2.3 SURFACE TEMPERATURE IP RETRIEVAL STRATEGY

Because the Surface Temperature IP is only used by the ice algorithms, it is only retrieved for regions within the Horizontal Coverage range of the ice ARPs and EDRs. An Ice Quality unit *[Y10881]* in the Snow/Ice module *[Y2477]* masks pixels outside of the range, de-weights pixels with cloud cover, and writes the results to an Ice Mask IP and an Ice Weights IP. Brightness temperatures for the two moderate resolution bands (M15 and M16) and for the one imagery resolution band (I5) are derived by the Radiometric Calibration unit of the Build-SDR module *[Y3261]*.

Two LUTs (Surface Temperature LUT and Spatial Weights LUT) are generated offline. These contain the parameters and weights required by the algorithm.

The surface temperature is computed at imagery resolution for all imagery pixels that are not masked and that have sufficient pixel weight, using the brightness temperatures of the I5, M15, and M16 bands. The split window algorithm is used where feasible. If there is bad M15 or M16 data, the single band algorithm is used.

A.3.0 ALGORITHM DESCRIPTION

A.3.1 PROCESSING OUTLINE

The unit process steps are:

1) Read the Ice Mask IP. If the mask contains a granule out of range flag, skip further processing and write a null IP.

2) Read the M15, M16, and I5 brightness temperatures from the SDRs.

3) Read the Cloud Mask IP, the Ice Weights IP, the AOT IP, the COT IP, and the PW IP, Use the information in these IPs to determine which imagery resolution pixels should be processed.

4) Read a correction switch from the BT Correction Switch LUT. If selected, correct the BTs for aerosol, thin cirrus, and PW effects.

5) Determine the brightness temperature differences D_k (= $(T11)_k$ - $(T12)_k$)) for each moderate resolution pixel (k), from the brightness temperatures in the M15 (T11) and M16 (T12) bands.

6) Determine the brightness temperature differences d_j (= $(t11)_j$ - $(t12)_j$)) for each good imagery resolution pixel (j) in the VIIRS granule, from the D_k of neighboring moderate resolution pixels, using spatial (Backus-Gilbert) weights obtained from a LUT.

7) Determine the quality of the brightness temperature differences d_j for each imagery resolution pixel (j) in the VIIRS granule, from the quality of the neighboring D_k.

8) Determine the brightness temperature equivalent to the M15 band at imagery resolution $(t11)_j$ for each imagery resolution pixel (j) in the VIIRS granule, using the observed brightness temperature in the I5 band (t_I), obtained from the VIIRS imagery resolution SDR, and applying a spectral fusion factor obtained from a LUT.

9) For all imagery resolution pixels with YELLOW or GREEN quality of d_j, apply the split window coefficients to t_{11} and t_{12} to determine surface temperature.

10) For all imagery resolution pixels with RED quality of d_j, apply the single-band coefficients to t_I to determine surface temperature.

11) Write the surface temperature and associated quality (GREEN, GREEN/YELLOW, YELLOW/RED, or RED) to the Surface Temperature IP file.

The unit level process flow is shown in Figure A-2.

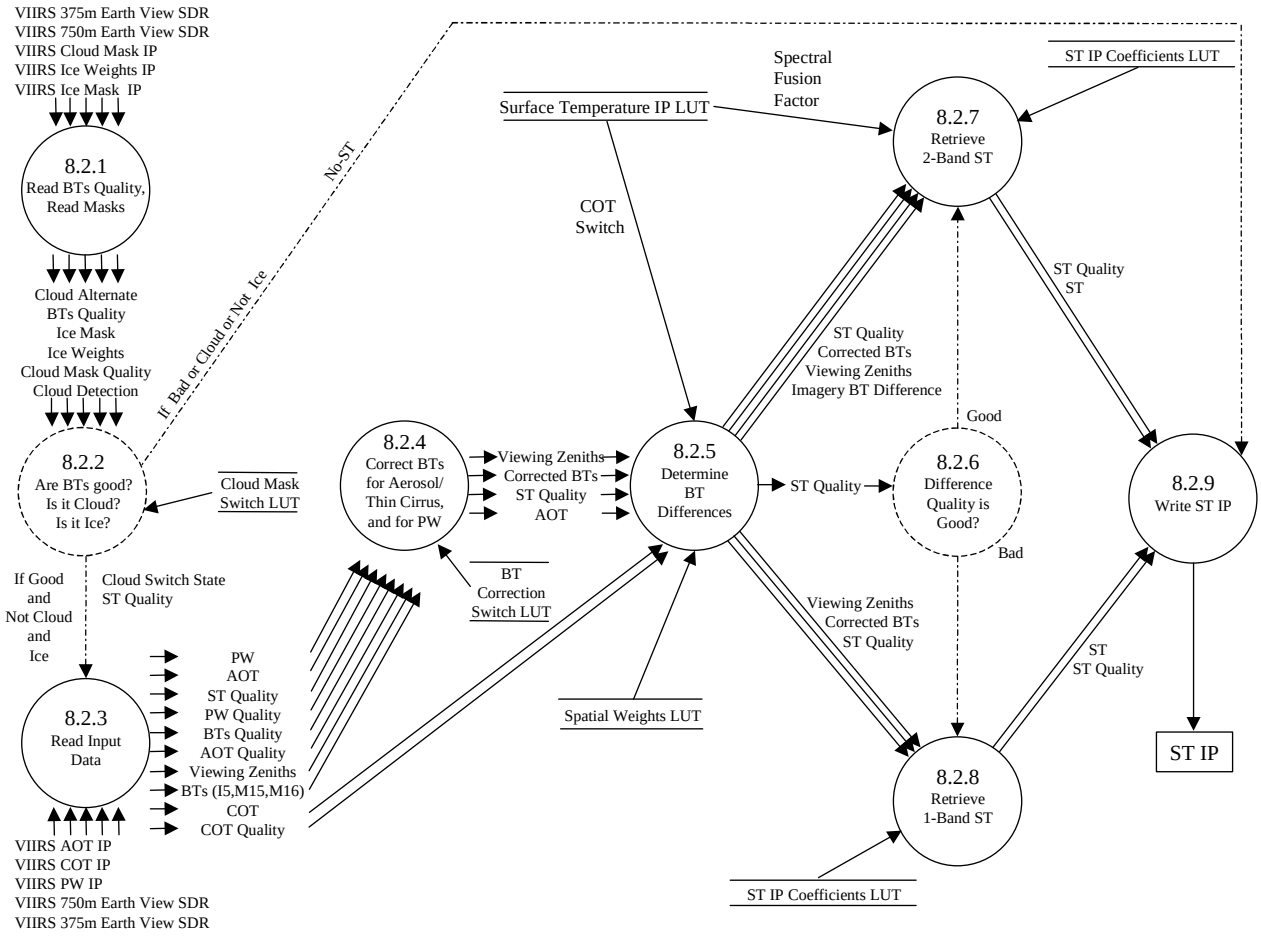

Figure A-2. VIIRS Surface Temperature IP Unit Level process flow

A.3.2 ALGORITHM INPUT

A.3.2.1 VIIRS Data

The VIIRS data presented in Table A-2 are required input to the algorithm processing code.

Table A-2. VIIRS data for the Surface Temperature IP

Input Data	Source of Data	Reference
Instrument (Band) Quality	VIIRS SDR	*[Y2479]*
Granule Range Flag	Ice Mask IP	*[Y10881]*
Brightness Temperature (M15, M16, I5)	VIIRS SDRs	*[Y2479], [Y3261]*
Solar/Sensor Angles	VIIRS SDRs	*[Y2479]*
Aerosol Optical Thickness (AOT)	Aerosol Optical Thickness IP	*[Y2471], [Y3277]*
Precipitable Water (PW)	Precipitable Water IP	*[Y3282]*
Cloud Mask	Cloud Mask IP	*[Y2412]*
Cloud Optical Thickness (COT)	Cloud Optical Thickness IP	*[Y2472], [Y3278]*
Surface Temperature IP Parameters	Surface Temperature IP LUT	*[Y10880]*
Surface Temperature Coefficients	ST IP Coefficients LUT	*[Y10880]*
Spatial Weights	Spatial Weights LUT	*[Y10880]*

Instrument (Band) Quality

The VIIRS EV_375M SDR will contain band I5 quality flags at imagery pixel resolution. Pixels with bad quality will not be processed. A RED quality flag will be set for these pixels. The VIIRS EV_750M SDR will contain band M15 and M16 quality flags at moderate pixel resolution. Imagery pixels nested within a moderate resolution pixel with bad quality will be processed by the fallback single band algorithm. A YELLOW quality flag will be set for these pixels.

Granule Range Flag

If the entire granule is out of the Horizontal Coverage range for all ice ARPs and EDRs, a granule range flag will be set in the Ice Mask IP. In that case, further processing of the granule will be bypassed. This will reduce the operational processing load, since most granules are out of range.

Brightness Temperatures

Brightness temperatures for the M15 and M16 bands are obtained from the VIIRS EV_750M SDR. Brightness temperatures for the I5 band are obtained from the VIIRS EV_375M SDR.

Solar / Sensor Angles

The VZA is used in the split window algorithm (Equation A-6).

Aerosol Optical Thickness

Aerosol optical thickness is used for BT correction.

Precipitable Water

Precipitable water is used for BT correction.

Cloud Mask

The VIIRS cloud mask *[Y2412]* is expected to derive a status of confident clear / probably clear / probably cloudy / confident cloudy for each pixel, building on MODIS cloud mask heritage (Ackerman *et al.*, 1997). Pixels classified as “cloudy” will be excluded from further processing. Pixels classified as “probably cloudy” are also expected to be excluded. This determination must depend on an assessment of the cloud mask performance, particularly over snow and ice surfaces. Pixels classified as “probably clear” or as “confident clear” will be processed. The cloud mask will also supply a thin cirrus flag, which may be used for BT correction.

Cloud Optical Thickness

Cloud optical thickness will be used as an alternative to the cloud mask. This will occur if a switch, obtained from the Surface Temperature IP LUT, is turned on.

Surface Temperature IP Parameters

A set of input parameters will be obtained from a pre-set VIIRS Surface Temperature IP LUT. The parameters also include a switch determining whether to use the Cloud Mask IP or the Cloud Optical Thickness IP for cloud masking, another switch determining whether or not to apply BT corrections, and a weight factor (spectral fusion factor) for combining the M15 and M16 BTs (c.f. Equation A-7).

Surface Temperature Coefficients

The coefficients used in the split window and single band algorithms will be obtained from a pre-set ST IP Coefficients LUT.

Spatial Weights

The spatial weights used for construction of the imagery resolution BT difference (Equation A-10) will be obtained from a pre-set Spatial Weights LUT.

A.3.2.2 Non-VIIRS Data

The algorithm requires no input data from outside the VIIRS system.

A.3.3 THEORETICAL DESCRIPTION OF SURFACE TEMPERATURE IP RETRIEVAL

A.3.3.1 Physics of the Problem

The physics of the IST retrieval are described in Section 3.3.1, in the EDR portion of this document.

A.3.3.2 Mathematical Description of the Algorithm

A.3.3.2.1 Split Window Regression

The VIIRS ST IP algorithm is based on statistical methods. Traditional statistical methods for satellite ST IP retrieval are linear multi-channel regression methods. The following regression methods are used in the VIIRS ST IP retrieval:

Split window (10.8 + 12 μm bands, from AVHRR method, Yu et al., 1995) (VIIRS ST IP baseline algorithm):

$$IST = a_o + a_1 T_{11} + a_2 (T_{11} - T_{12}) + a_3 (\sec(z) - 1) \quad \text{(A-1)}$$

One channel (12 μm band). (VIIRS ST IP fallback algorithm):

$$IST = a_o + a_1 T_{12} + a_2 (\sec(z) - 1) \quad \text{(A-2)}$$

Satellite-measured radiance is a function of the atmospheric profiles and surface properties. For the IR window and water vapor channels, the radiance over oceans at the top of the atmosphere is mainly a function of the surface temperature and the temperature and moisture profiles. One can choose a few channels (e.g., 3 channels) for which only the main structures of the temperature and moisture profiles are required to obtain ice surface temperature.

A.3.3.2.2 Calibrated TOA Brightness Temperatures

The blackbody radiance (R) function is

$$R = 2 h \nu^3 / [c^2 (\exp\{-h\nu/kT\} - 1)] \quad \text{(A-3)}$$

where ν is the wavenumber (cm^{-1}), h is the Planck constant, c is the speed of light, k is Boltzman's constant, and T is the temperature in Kelvin.

Equation A-3 can be written as

$$R = c_1 \nu^3 / [c^2 (\exp\{-c_2 \nu / T\} - 1)] \quad \text{(A-4)}$$

where c_1 and c_2 are two blackbody constants equal to 0.01191071 and 1.438838 respectively using cgs units.

This can be solved for the brightness temperature (T or T_b) to give:

$$T_b = c_2 \nu / \ln(1 + c_1 \nu^3 / R) \quad \text{(A-5)}$$

A.3.3.2.3 Fusion with Imagery Resolution Band

Note: In the following equations, we use a convention whereby quantities at imagery resolution are designated with lower case characters, quantities at moderate resolution are designated with upper case characters, and observed quantities are in bold font.

The purpose of achieving a fusion of the moderate resolution brightness temperatures with the imagery resolution brightness temperature is to be able to apply the split window algorithm at imagery resolution:

$$st = a_o + a_1 t_{11} + a_2 (t_{11} - t_{12}) + a_3 (\sec(\boldsymbol{z}) - 1) \quad \text{(A-6)}$$

where:

t_{11} = M15 brightness temperature (K) at imagery resolution

t_{12} = M16 brightness temperature (K) at imagery resolution

In equation A-6, the $_{11}$ and $_{12}$ subscripts for the M15 and M16 bands are used to match the terms in the ST IP split window algorithm (Equation A-1) and the regression coefficients are identical to those for the IST algorithm.

To apply equation A-6, we must derive t_{11} and t_{12}, which are not directly observable by the VIIRS bands. To solve for these two unknowns, we use the observed brightness temperatures in the M15, I5, and M16 bands, and make the following assumptions:

1) The brightness temperature in the LWIR imagery band (I5) can be written as a linear combination of the brightness temperatures in the moderate resolution LWIR bands (M15 and M16):

$$\mathbf{t_I} = f\, t_{11} + (1- f)\, t_{12} \qquad \text{(A-7)}$$

where:

t_I = I5 brightness temperature (K) at imagery resolution

and the spectral fusion factor, f, which is defined by equation A-7, is in general a function of R, the source radiance spectrum.

The spectral fusion factor can be rigorously determined from the spectral response functions, as part of the calibration process. In practice, it may be sufficient to determine it analytically from equation A-5, using the band centers and band radiances for each of the three bands:

$$f = (t_I - t_{12}) / (t_{11} - t_{12}) \qquad \text{(A-8)}$$

where:

$$t_I = c_2\, \nu_I / \ln(1 + c_1\, \nu_I^3 / R_I) \text{ , etc.} \qquad \text{(A-9)}$$

2) The brightness temperature difference, $t_{11} - t_{12}$, is primarily determined by atmospheric conditions that are stable on a spatial scale of a few km. This allows us to reliably approximate the brightness temperature difference at imagery resolution as a linear combination of the differences in the neighboring moderate resolution pixels:

$$d = \Sigma\, \mathbf{D_k}\, w_k / \Sigma\, w_k \qquad \text{(A-10)}$$

where:

$$d = t_{11} - t_{12} \qquad \text{(A-11)}$$

= brightness temperature difference for the imagery resolution pixel

$$\mathbf{D}_k = \mathbf{T}_{11} - \mathbf{T}_{12} \quad \text{(A-12)}$$

= brightness temperature difference for moderate resolution pixel (k)

w_k = relative weight of moderate resolution pixel (k).

and the sum is over all neighboring moderate resolution pixels with non-zero weight.

To determine the relative weights of the neighboring pixels, we adopt the Backus-Gilbert method for constructing a desired spatial response function from a set of neighboring spatial response functions.

A.3.3.2.4 Backus-Gilbert Construction

Backus and Gilbert (1970) developed a method for approximating a given function as a linear combination of other functions, in the context of inversion of seismic signals propagated through the Earth. The idea of applying the Backus-Gilbert method to the microwave radiometer deconvolution problem was first suggested by Stogryn (1978), and has been applied to the analysis of Special Sensor Microwave Imager (SSM/I) data (Poe, 1990; Farrar and Smith, 1992; Robinson, Kummerow, and Olson, 1992; Farrar, Smith, and Xiang, 1994). The method will be used as part of the algorithm to produce Advanced Microwave Scanning Radiometer (AMSR) Level 2A products (Ashcroft and Wentz, 1998). The application to microwave data attempts to correct for the effects of the antenna pattern on the measured microwave signal. Most of the following description is taken from Stogryn (1978).

Consider a radiometer observing the earth from a satellite. If the bore-sight direction of the antenna is specified by the unit vector $\mathbf{s_0}$, then the antenna temperature $T_A(\mathbf{s_0})$ is given by:

$$T_A(\mathbf{s_0}) = \int G(\rho, \mathbf{s_0})\, T_B(\rho)\, d\Omega \quad \text{(A-13)}$$

where ρ is a unit vector from the antenna in the direction of the solid angle, $G(\rho, \mathbf{s_0})$ is the antenna gain function, (antenna pattern), normalized so that:

$$\int_{4\pi} G(\rho, \mathbf{s_0})\, d\Omega = 1 \quad \text{(A-14)}$$

and the integration is over all solid angles with a significant signal T_B.

Suppose now that a sequence of antenna temperature measurements are made for a number of different beam directions $\mathbf{s_0}$ with the purpose of deducing $T_B(\rho)$. For the *ith* measurement, equation (A-13) will hold with $\mathbf{s_0} = \mathbf{s_{0i}}$. So, we can re-write equation (A-13) as:

$$T_A(i) = \int G_i(\rho)\, T_B(\rho)\ d\Omega \qquad \text{(A-15)}$$

where $G_i(\rho) = G(\rho, \mathbf{s_{0i}})$.

If N measurements are made, the N functions $G_i(\rho)$ (i = 1,…,N) may be considered known since they depend only on the specified scan/track geometry and antenna patterns.

The problem of determining $T_B(\rho_0)$ for a given line of sight ρ_0 from the N measurements is mathematically identical to the problem treated by Backus and Gilbert (1970). The method consists in seeking a linear combination of the measurements which approximates $T_B(\rho_0)$ according to some objective criterion. If we write:

$$T_B(\rho_0) = \Sigma\, a_i\, T_A(i) \quad , \quad (i = 1,N) \qquad \text{(A-16)}$$

where the constants a_i are to be determined, we derive by substitution in equation (A-15):

$$\Sigma\, a_i\, T_A(i) = \int \left[\Sigma\, a_i\, G_i(\rho)\right] T_B(\rho)\ d\Omega \qquad \text{(A-17)}$$

If the bracketed term in equation (A-17) were the delta function $\delta(\rho - \rho_0)$, then equation (A-16) would be an exact solution of the problem. However, with a finite number of measurements, it is not possible to choose the a_i to produce the delta function. An approximation which most closely produces some desired behavior is sought. Stogryn (1978) suggested the minimization of the function:

$$Q = Q_0 \cos(\gamma) + e^2\, w \sin(\gamma) \qquad \text{(A-18)}$$

where: $$Q_0 = \int \left[(\Sigma\, a_i\, G_i(\rho)) - F(\rho, \rho_0),\right]^2\ J(\rho, \rho_0)\ d\Omega \qquad \text{(A-19)}$$

and: $$e^2 = \mathbf{a}^T \boldsymbol{E}\ \mathbf{a} \qquad \text{(A-20)}$$

In this formulation, **a** is the column vector whose components are a_i, $\boldsymbol{E}$ is the error covariance matrix of the measurements, and F and J are specified functions. The terms w and γ are used to balance the effects of resolution and noise in the solution. Ashcroft and Wentz (1998) adopt this approach for AMSR. They combine w and γ into a single term, $\beta = w \tan(\gamma)$, to re-write equation (A-18) as:

$$Q = Q_0 + e^2\, \beta \qquad \text{(A-21)}$$

Minimization of Q, with the constraint:

$$\int \left[\Sigma\, a_i\, G_i(\rho)\right]\ d\Omega = 1 \qquad \text{(A-22)}$$

and non-negative β, provides the a_i from which the desired brightness temperature is computed by equation (A-16).

The Backus-Gilbert method will construct the brightness temperature for a desired pixel, using the brightness temperatures of the measurements in the neighborhood of that pixel:

$$T_B = \Sigma\, a_i\, T_B(i) \quad , \quad (i = 1,N) \tag{A-23}$$

Where the a_i are Backus-Gilbert coefficients. These are computed by minimization of the term Q in equation (A-21), subject to the constraint in equation (A-22).

The coefficients are computed for each channel as:

$$\mathbf{a} = \boldsymbol{S}^{-1} \left[\mathbf{v} + \mathbf{u} \left(1 - \mathbf{u}^T \boldsymbol{S}^{-1} \mathbf{v}\right) / \left(\mathbf{u}^T \boldsymbol{S}^{-1} \mathbf{u}\right) \right] \tag{A-24}$$

where:

$$u_i = \int G_i(\rho)\, d\Omega \qquad (i=1,N) \tag{A-25}$$

$$v_i = \int G_i(\rho)\, F(\rho)\, J(\rho)\, d\Omega \qquad (i=1,N) \tag{A-26}$$

$$G_{ij} = \int G_i(\rho)\, G_j(\rho)\, J(\rho)\, d\Omega \qquad (i=1,N;\ j=1,N) \tag{A-27}$$

$$S_{ij} = G_{ij} + \beta\, \sigma^2\, \delta_{ij} \qquad (i=1,N;\ j=1,N) \tag{A-28}$$

The integrals are centered at the synthesized cell center, and are with respect to the angle at the sensor:

$$\int d\Omega = \int d\phi \int \sin(\rho)\, d\rho = 2\pi \int \sin(\rho)\, d\rho \tag{A-29}$$

where ρ is the angular offset ($\rho = 0$ at the synthesized cell center). Note that the equations assume that the functions are circularly symmetric, i.e. independent of ϕ.

The $\mathbf{G_i(\rho)}$ are the band spatial response functions. For the initial analysis, we will use Gaussian point spread functions:

$$G(\rho) = A \,/\, \exp[(\rho/B)^2] \tag{A-30}$$

where B is selected from sensor models for each band, and A is selected so that

$$\int G(\rho)\, d\Omega = 1 \tag{A-31}$$

During the EDU fabrication phase, we can use measured EDU spatial response functions.

$\mathbf{F(\rho)}$ is the desired spatial response function, which we will refer to as the reference function. We wish to produce the brightness temperature that would be observed if the sensor's spatial response function was $F(\rho)$. For our purposes, $F(\rho)$ is the response function for band I5. For the initial analysis, we use a Gaussian with imagery resolution Horizontal Spatial Resolution (HSR).

For the initial analysis, we use a Gaussian with moderate resolution HSR as a reference pattern (G). Our goal is to construct brightness temperatures by applying Backus-Gilbert coefficients to source brightness temperatures obtained from reference pattern G, and minimize the difference between the constructed brightness temperatures and the brightness temperatures obtained from response function F. During the EDU fabrication phase, we will consult with the VIIRS contractor to decide upon the desired form for the reference pattern.

J(ρ**)** is a tuning function. For our purposes, we set it equal to unity, following AMSR practice.

σ^2 is the channel RMS noise variance. For the initial analysis, we will set this to zero. During the EDU fabrication phase, we will use measured EDU channel noise. Note that we have approximated the measurement error covariance matrix as $e^2 = \sigma^2 \delta_{ij}$. If subsequent analysis of the EDU characteristics warrants the inclusion of off-diagonal terms, we will add them.

β is a resolution/noise balance factor. For the initial analysis, this factor is not relevant, as the noise is set to zero. During the EDU fabrication phase, we will run simulations to optimize β.

δ_{ij} is the Kronecker delta function (=1, if i equals j; =0, if i is not equal to j).

Figure A-3 shows a schematic of the construction for the N=3 case.

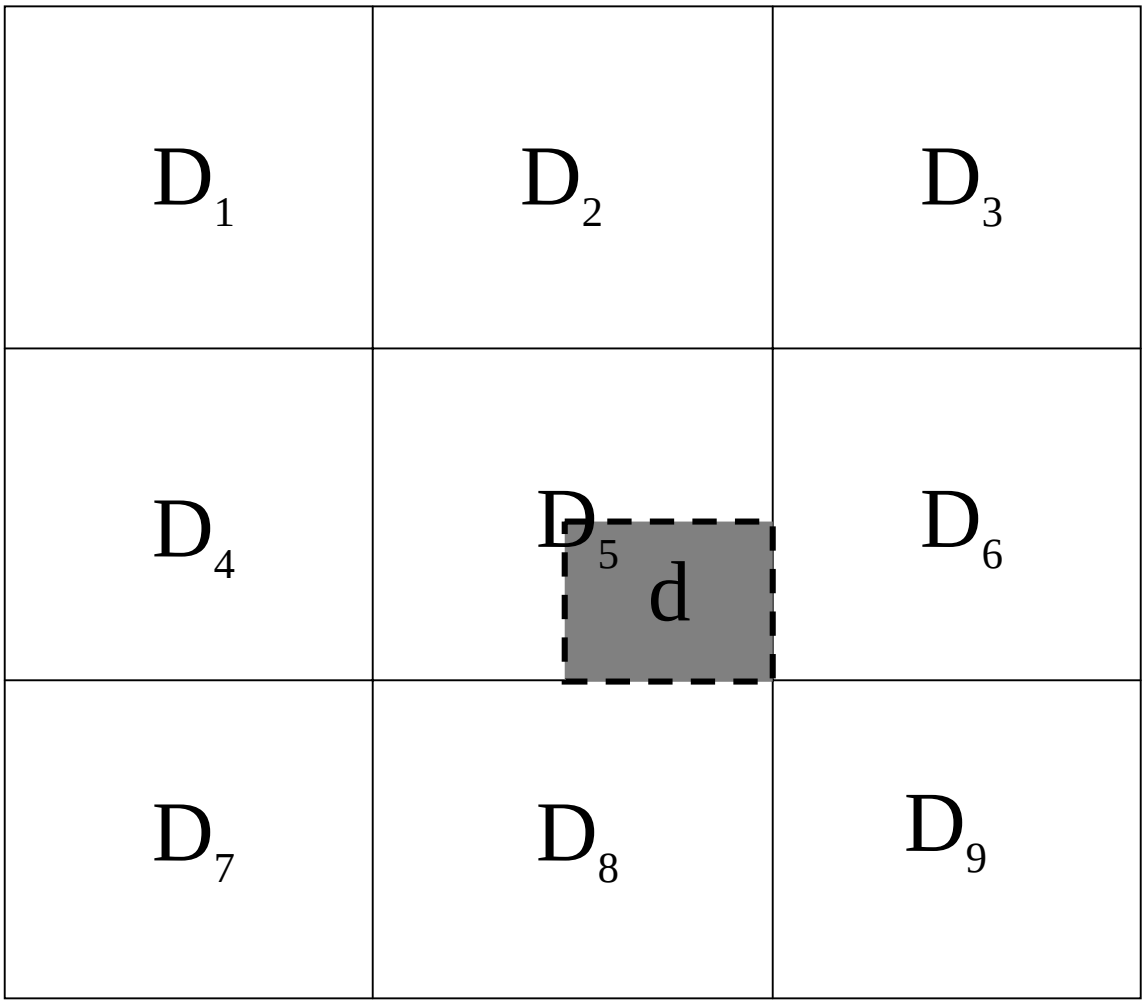

Figure A-3. Schematic of Backus-Gilbert constructed brightness temperature difference for the N=3 case

In the figure, the brightness temperature difference ($d = t_{11} - t_{12}$) for the indicated imagery resolution pixel, is computed as the weighted mean of the observed brightness temperature differences ($D_k = (T_{11})_k - (T_{12})_k$; k=1,9) of the nine nearest moderate resolution pixels. Because the imagery pixels are nested 2x2 with the moderate resolution pixels everywhere along the scan and across the scan, this geometry is applicable for all pixels in a VIIRS granule.

In the case that one or more of the neighboring moderate resolution pixels contains bad data for M15 or M16, the Backus-Gilbert construction is bypassed, and d is set equal to D for the central pixel (D_5 in the figure). A quality flag is attached to each of the four imagery resolution pixels nested in the central pixel. In the case that the central pixel contains bad data for M15 or M16, the single band algorithm is applied to each of the four imagery resolution pixels nested in the central pixel, and a quality flag is attached to each of the pixels.

A.3.3.3 Single Band Fallback

The split window algorithm cannot be applied if the M15 or M16 data are bad. In that case, a single band algorithm will be applied:

$$st = a_o + a_1 t_1 \quad \text{(A-32)}$$

and a quality flag will be attached.

A.3.3.4 Archived Algorithm Output

Surface Temperature will be produced at imagery resolution as the Surface Temperature IP. The IP is used as input to the VIIRS Ice Concentration software unit *[Y3235]*. It can be archived as a P^3I product. Currently, the IP will not be written for pixels outside of the Horizontal Coverage range for sea ice or fresh water ice. If there is interest in a P^3I product outside of the ice zones, the algorithm can be implemented over a wider region.

A.3.3.5 Variance and Uncertainty Estimate

The Surface Temperature IP is not a system level requirement and therefore does not have a system specification. Surface Temperature IP performance requirements are this driven by the system specifications for the sea ice and fresh water ice products. Surface temperature IP errors were estimated in Phase I as part of the error budget process for the Imagery Sea Ice products *[Y2466]* and Fresh Water Ice EDR *[Y2404]*. Performance estimates were derived as follows:

The split-window Ice Surface Temperature algorithm was applied to MODIS Airborne Simulator (MAS) scenes at a 50 meter pixel resolution. Brightness temperatures in MAS bands 45 (11 μm) and 46 (12 μm) were calculated from the unperturbed TOA radiances in those bands, and used as input data to the algorithm. The retrieved surface temperatures were adopted as "truth". The 50 meter truth was aggregated to VIIRS imagery pixel sizes at nadir (8 x 8 aggregation to 0.4 km pixels). The aggregated temperatures were adopted as VIIRS "truth".

The MAS TOA radiances were then aggregated to VIIRS pixel size. A proxy for the VIIRS I5 band radiance was made from the average of the band 45 and 46 radiances. The VIIRS model radiances were perturbed by our models for sensor noise and calibration bias. A 0.5% calibration bias was applied to all radiances. Sensor noise models for VIIRS bands M15 (11 μm), M16 (12 μm), and I5 (11.45 μm) were applied to the corresponding radiances. The perturbed radiances were converted to brightness temperature, and used as input data to the Surface Temperature IP algorithm.

Surface Temperature IP accuracy, precision, and uncertainty errors were calculated from comparison of the retrieved surface temperature to the "truth". At nadir, these errors are 0.278 K in accuracy and 0.378 K in precision. At edge of scan, the precision error is 0.508 K.

It may seem at first glance that this performance is much better than would be expected from the NEdT specification for the I5 band (c.f. Table A-1). There are two reasons for this:

1) The NEdT specification for band I5 is at a reference temperature (Ttyp) of 210K. Surface temperatures in regions where we need performance (the marginal ice zones) are ~ 270K, where NEdT is significantly smaller.

2) NEdT performance is better than specification, since our specification includes margin.

NEdT performance for the three thermal bands used by the algorithm is shown in Figure A-4.

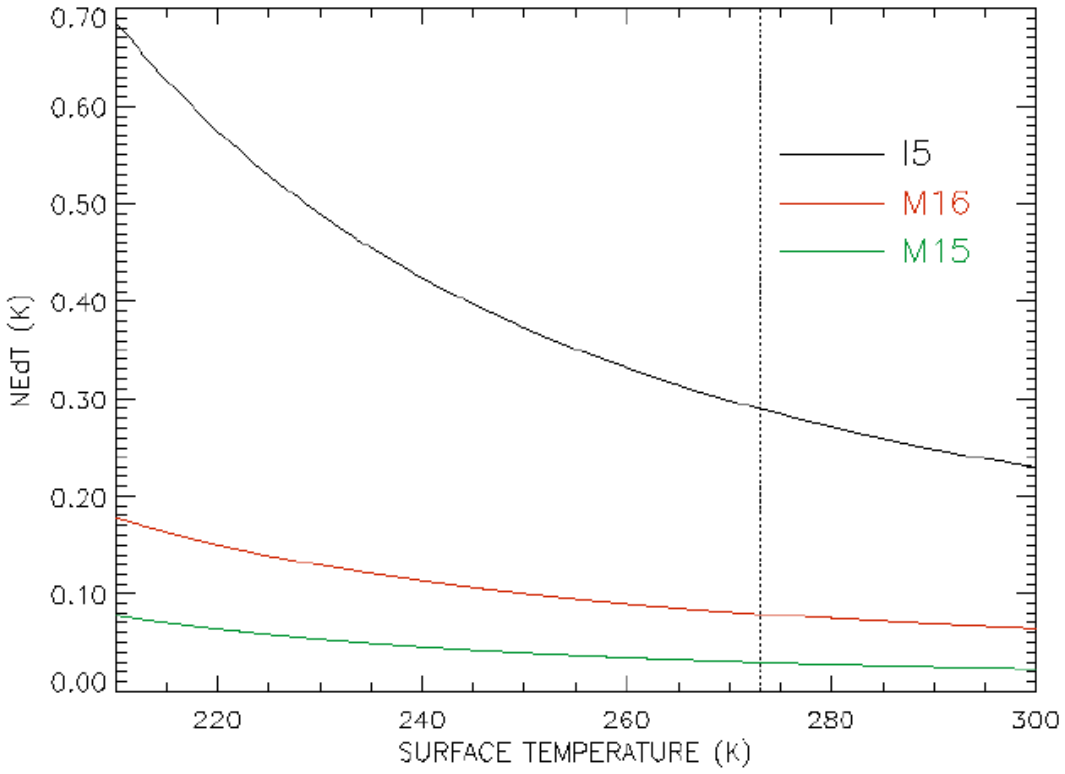

Figure A-4. NEdT performance estimates for bands I5, M15, and M16

At the ice/water temperature boundary (~ 273 K, indicated by the vertical dotted line in the figure), band I5 NEdT performance is 0.289 K. This is somewhat smaller than our derived precision error in Phase I (0.378K at nadir). We assume that the additional derived error is due to band misregistration and/or atmospheric variance, and that the error derived in Phase I from MAS data is still a good estimate of the Surface Temperature IP error in the marginal ice zones.

A.3.4 ALGORITHM SENSITIVITY STUDIES

We identify the following factors as possibly contributing to the total error budget for the Surface Temperature IP

- Sensor noise
- Calibration
- MTF
- Band Registration
- Atmospheric Correction

Sensor Noise: Sensor noise is characterized by the NEdT, as discussed in Section A.3.3.5.

Calibration: We applied a calibration bias of 0.5% to the brightness temperature, as discussed in Section A.3.3.5.

MTF: MTF smearing of the radiances will alias real horizontal variability into errors in measured reflectance and/or temperature for a given pixel. We have not quantified this error yet. Our sensitivity study with the MAS scene (Section A.3.3.5) will have included MTF effects in the total measured error.

Band Registration: Band-to-band registration errors will also alias horizontal variability into measurement error. These errors only apply to the split window retrieval, which uses more than one band. Our sensitivity study with the MAS scene (Section A.3.3.5) will have included band misregistration effects in the total measured error. If band misregistration is determined to be a significant error source, we can always use the single band algorithm. Such a determination will have to await validation with actual NPOESS Preparatory Program (NPP)/VIIRS data.

Atmospheric Correction: Atmospheric correction errors are typically perturbations in derived brightness temperature caused by water vapor and aerosols. These errors, discussed in Section 3.3.4, are generally not expected to be important for most cases of retrievals in polar regions. An additional source of atmospheric error is the aliasing of water vapor spatial variability with the error in the Backus-Gilbert constructed BT difference. A construction error is unavoidable, since no finite set of spatial weights can completely construct the correct spatial response function. Although we do not expect this error to be important, we recommend that the appropriate sensitivity study be conducted in the future, following the derivation of spatial weights from the measured VIIRS EDU spatial response functions, using MAS data.

A.3.5 PRACTICAL CONSIDERATIONS

A.3.5.1 Numerical Computation Considerations

Because all coefficients are pre-computed and stored in LUTs, the algorithm will run quickly and efficiently.

A.3.5.2 Programming and Procedural Considerations

The algorithm requires data from the Build SDR Module, the Snow/Ice Module, the Aerosol Module, and the Cloud Module.

A.3.5.3 Quality Assessment and Diagnostics

Pixel-based quality flags (TBD) will be provided which indicate the confidence in the IP. These will include RED flags for pixels containing bad data.

A.3.5.4 Exception Handling

The process will apply the pre-computed coefficients for all imagery resolution pixels containing good data. In the case that the co-spatial moderate resolution pixel contains bad data, the algorithm will apply the single band algorithm, and flag the pixel. In the case that neighboring moderate resolution pixels are bad, the process will use the brightness temperature difference of the co-spatial moderate resolution pixel in place of the Backus-Gilbert construction, and will flag the pixel.

A.3.6 ALGORITHM VALIDATION

A.3.6.1 Pre-Launch Validation

Pre-launch validation of the IST algorithms has been discussed in Section 3.6.1. Validation of the additional spectral and spatial functions used by the ST IP algorithm will be made from VIIRS EDU observed properties.

A.3.6.2 Post-Launch Validation

Post-launch validation of the IST algorithms has been discussed in Section 3.6.2. Validation of the additional spectral and spatial functions used by the ST IP algorithm will be made from NPP/VIIRS data.

A.4.0 ASSUMPTIONS AND LIMITATIONS

The ST IP algorithm is subject to the same assumptions and limitations as the IST algorithm (Section 4.0 of this document). The only additional assumption is that the water vapor correction at imagery resolution is sufficiently close to the correction at moderate resolution. By sufficiently close, we mean that the additional error caused by variation in water vapor on a spatial scale less than ~ 1km is small compared with the error in the split window IST retrieval. This assumption will be tested with MAS data.

A.5.0 REFERENCES

Ashcroft, P. and F.J. Wentz (1998),"AMSR Level 2A Algorithm Theoretical basis Document (ATBD)," Remote Sensing Systems Tech. Report 121599B.

Backus, G. and F. Gilbert (1970), "Uniqueness in the Inversion of Inaccurate Gross Earth Data," *Phil. Trans. Roy. Soc. London, Vol. A266,* 123-192.

Berk, A., L. S. Bemstein, and D. C. Robertson (1987). MODTRAN: A moderate resolution model for LOWTRAN. Rep. GLTR-89-0122, Burlington, MA: Spectral Sciences, Inc.

Cornette, W. M., P. K. Acharya, D. C. Robertson, and G. P. Anderson (1994). Moderate spectral atmospheric radiance and transmittance code (MOSART). Rep. R-057-94(11-30), La Jolla, CA: Photon Research Associates, Inc.

Farrar, M.R. and E.A. Smith (1992), "Spatial Resolution Enhancement of Terrestrial Features Using Deconvolved SSM/I Microwave Brightness Temperatures," *IEEE Transactions on Geoscience and Remote Sensing, Vol. 30, No. 2,* 349-355.

Farrar, M.R., E.A. Smith, and X. Xiang (1994), "The Impact of Spatial Resolution Enhancement of SSM/I Microwave Brightness Temperatures on Rainfall Retrieval Algorithms," *J. Applied Meteorology, Vol. 33,* 313-333.

Kneizys, F. X., E. P. Shettle, L. W. Abreu, J. H. Chetwynd, G. P. Anderson, W. O. Gallery, J. E. A. Selby, and S. A. Clough (1988). Users guide to LOWTRAN7. Rep. AFGL-TR-88-0177, Bedford, MA: Air Force Geophys. Lab.

Poe, G.A. (1990), "Optimum Interpolation of Imaging Microwave Radiometer Data," *IEEE Transactions on Geoscience and Remote Sensing, Vol. 28, No.5,* 800-810.

Robinson, W.D., C. Kummerow, and W.S. Olson (1992), "A Technique for Enhancing and Matching the Resolution of Microwave Measurements from the SSM/I Instrument," *IEEE Transactions on Geoscience and Remote Sensing, Vol. 30, No.3,* 419-429.

Stogryn, A. (1978), "Estimates of Brightness Temperatures from Scanning Radiometer Data," *IEEE Transactions on Antennas and Propagation, Vol. AP-26, No. 5,* 720-726.

Yu, Y., D. A. Rothrock, and R. W. Lindsay (1995). Accuracy of sea ice temperature derived from the advanced very high resolution radiometer. *J. Geophys. Res.*, 100, 4525-4532.